

Article

Transportational Cyclic Steps Created by Submarine Long-Runout Turbidity Currents

Zhuyuan Wu ^{1,*} and Norihiro Izumi ^{2,†}

¹ Graduate School of Engineering, Hokkaido University, Kita 13-jo Nishi 8-chome, Kita-ku, Sapporo 060-8628, Japan

² Faculty of Engineering, Hokkaido University, Kita 13-jo Nishi 8-chome, Kita-ku, Sapporo 060-8628, Japan; nizumi@eng.hokudai.ac.jp

* Correspondence: wuzhuyuan@eis.hokudai.ac.jp

† These authors contributed equally to this work.

Abstract: In recent years, it has become a common understanding among researchers that one of the significant agents for forming a variety of submarine geomorphologies is turbidity currents that travel long distances, so-called long-runout turbidity currents. In this study, we present a mathematical model of the formation of cyclic steps due to long-runout turbidity currents based on the assumption that the highly concentrated layer near the bottom of the turbidity currents achieves an equilibrium state. The model uses the four governing equations: the momentum equation, the continuity equation, the diffusion/dispersion equation of suspended sediment, and the continuity equation of sediment on the bed (the Exner equation). We simplify the governing equations by ignoring the entrainment from ambient water since there is a distinct density interface above the highly concentrated lower layer of long-runout turbidity currents. We determine the dimensions of cyclic steps based on the solution. Agreement between the predictions and field observations turns out to be reasonable.

Keywords: bedforms; cyclic steps; sediment transport; suspended sediment; turbidity currents



Citation: Wu, Z.; Izumi, N.

Transportational Cyclic Steps Created by Submarine Long-Runout Turbidity Currents. *Geosciences* **2022**, *12*, 263. <https://doi.org/10.3390/geosciences12070263>

Academic Editors: Pedro J.M. Costa and Jesus Martinez-Frias

Received: 19 May 2022

Accepted: 27 June 2022

Published: 29 June 2022

Publisher's Note: MDPI stays neutral with regard to jurisdictional claims in published maps and institutional affiliations.



Copyright: © 2022 by the authors. Licensee MDPI, Basel, Switzerland. This article is an open access article distributed under the terms and conditions of the Creative Commons Attribution (CC BY) license (<https://creativecommons.org/licenses/by/4.0/>).

1. Introduction

Cyclic steps are a series of upstream migrating steps bounded by hydraulic jumps. The flow is subcritical at the stoss side, where the slope is gentle, and the flow accelerates on the lee side to become supercritical flow. Taki and Parker [1] performed detailed experiments, regenerated the cyclic steps in the laboratory, and found the steps migrate upstream while preserving their form. We observe cyclic steps on the ocean floor [2,3], at river deltas [4], and on ice [5], classified into three types: transportational [1,6], net-erosional [7], and net-depositional [8]. In our study, we focus on submarine transportational cyclic steps, such as cyclic steps within the South Taiwan Shoal and West Penghu submarine canyons of the South China Sea [9].

The increased research interest in cyclic steps is due to their effect on geomorphology and a new awareness of the vital role in sediment transport efficiency. There are many models proposed previously for describing the formation of cyclic steps. Parker and Izumi [7] presented a model to analyze purely erosional cyclic steps on cohesive soil in open channel flow. Sun and Parker [6] developed an analytical model for transportational cyclic steps formed in open channel flow with abundant suspended sediment. Izumi and Yokokawa [10] performed a theoretical analysis to explain the formation of cyclic steps in mixed bedrock–alluvial channels. As for cyclic steps formed due to turbidity currents in submarine environments, Dias et al. [11] have proposed the first analytical model, to the authors' knowledge. Their model used variables in the critical regime in the Froude sense to normalize all the main variables, such as the layer thickness of turbidity currents. Therefore, it is not easy to interpret their results in reality and compare the dimensions of cyclic steps predicted by their model with those in the field.

In many cases, turbidity currents lead to the formation of cyclic steps. Turbidity currents are sediment gravity flows triggered by slumping, earthquakes, and various other types of soil disturbances. Many analytical models have been presented in the endeavor to understand turbidity currents. Parker et al. [12] proposed a three-equation model and a four-equation model, which includes the turbulent kinetic energy equation to describe the behavior of turbidity currents. The entrainment from ambient water included in the two models leads to the thickening of currents. Izumi [13] combined the model of turbidity currents and the Exner equation to reproduce the formation of submarine gullies due to turbidity currents.

A remarkable feature of submarine turbidity currents is that they can run over 1000 km without dissipation. The models proposed by Parker et al. [12] have a limitation: they cannot explain this feature of long-runout turbidity currents. The physical mechanism of why turbidity currents can travel long distances had long been left unsolved. Luchi et al. [14] are the first to suggest a solution to this problem. In the process of deriving the velocity distribution of turbidity currents in the layer thickness direction using the $k-\epsilon$ model, they found that the turbidity current separates into two layers: a lower layer with high suspended sediment concentration and an upper layer with low suspended sediment concentration. This separation creates a density interface between the upper and lower layers where there are very little friction, momentum exchange, and diffusion. Since there is very little friction between the two layers, the lower layer has little interaction with the upper layer and can run long distances. The recent field observations by Paull et al. [15] and Pope et al. [16] partly support this assumption that a turbidity current is composed of two layers.

Earlier models designed to generate submarine morphologies failed to describe the characteristic of long-runout turbidity currents. Hence, in our study, one of the objectives was to capture the features of these currents. We derive the governing equations for long-runout turbidity currents in a manner consistent with that used by Parker et al. [12]. However, we establish the governing equations by integrating over the highly concentrated lower layer of turbidity currents based on the model of Luchi et al. [14] rather than from the bottom to infinity. We coupled with the governing equations of long-runout turbidity currents and the Exner equation as in the model by Dias et al. [11] and Izumi [13]. Taki and Parker [1] have studied the subaqueous equivalent of submarine cyclic steps and found that cyclic steps migrate upstream without changing their forms. We referred to the method presented by Sun et al. [6] to solve this problem of cyclic steps formed by long-runout turbidity currents in submarine environments.

Models proposed so far to describe cyclic steps, e.g., ref. [6] have not explained the actual scale of cyclic steps. Therefore, we normalize all the variables by the fundamental quantities in the absence of steps such as the equilibrium thickness of the highly concentrated lower layer and then calculate the actual dimensions of cyclic steps using the results of the analysis performed by Izumi [17]. We then compare these results with observations in the field to determine the reliability of our model.

2. Materials and Methods

2.1. Formulation

2.1.1. Governing Equations

Turbidity currents continually entrain ambient water. As a result, increased layer thickness results in the dilution of suspended sediment concentration. Some turbidity currents can run incredibly long distances without dissipating. As already mentioned, Luchi et al. [14] found that this feature of turbidity currents results from the fact that the flow separates into two layers, as shown in Figure 1.

The lower driving layer has the invariant suspended sediment concentration, flow thickness, and velocity profiles, while the upper driven layer continues to entrain neighboring water and become diluted.

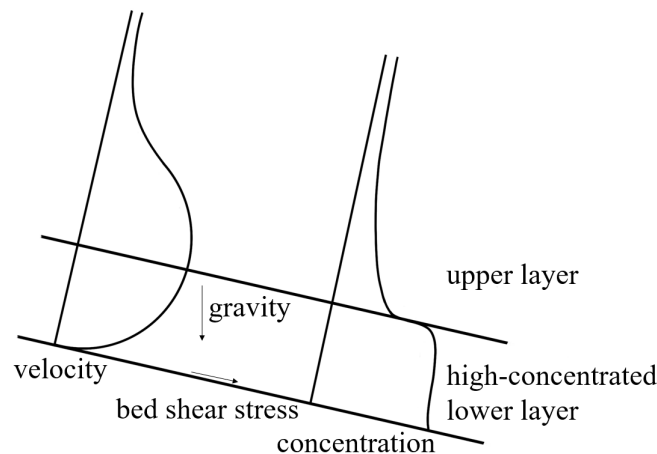


Figure 1. Sketch of the model.

There is a distinct density interface between the two layers, where the velocity gradient and the shear stress are almost zero. The gravity drives the upper layer and balances the shear stress at the bottom of the lower layer. We can assume that the highly concentrated lower layer is in the equilibrium state in this configuration.

We adopt the derivation of the layer-averaged equations in the model by Parker et al. [12] in this study. However, the integration approach of the governing equations is slightly different: in this study, we integrate the governing equations over the highly concentrated lower layer. Even after this manipulation, however, the layer-averaged momentum equation has the same form as that achieved in the model presented by Parker et al. [12]

$$\tilde{U} \frac{\partial \tilde{U}}{\partial \tilde{x}} = -\frac{Rg}{2} \tilde{h} \frac{\partial \tilde{C}}{\partial \tilde{x}} - Rg\tilde{C} \frac{\partial \tilde{h}}{\partial \tilde{x}} - Rg\tilde{C} \frac{\partial \tilde{\eta}}{\partial \tilde{x}} + Rg\tilde{C}S - \frac{\tilde{\tau}_b}{\rho\tilde{h}} \tag{1}$$

where \tilde{x} is the streamwise coordinate, \tilde{U} is the layer-averaged flow velocity in the \tilde{x} direction, \tilde{C} is the layer-averaged suspended sediment concentration, \tilde{h} is the highly concentrated layer thickness of turbidity currents, R is the submerged specific gravity, g is the gravity acceleration, $\tilde{\eta}$ is the deviation from the bed elevation without steps, S is the average slope, ρ is the density of water, and $\tilde{\tau}_b$ is the bed shear stress ($=\rho c_D \tilde{U}^2$), and c_D is the drag coefficient. In addition, we denote dimensional variables by the tilde and drop it to denote non-dimensional or normalized equivalents.

The layer-averaged continuity equation is

$$\frac{\partial \tilde{U}\tilde{h}}{\partial \tilde{x}} = 0 \tag{2}$$

Note that the right-hand side of Equation (2) vanishes, whereas it does not in the model proposed by Parker et al. (1986), that is $e_w \tilde{U}$, where e_w is the entrainment rate of water. Since we only consider the highly concentrated layer of turbidity currents, the entrainment from ambient water is assumed to be negligible.

The layer-averaged dispersion/diffusion equation of suspended sediment is described by

$$\frac{\partial \tilde{U}\tilde{C}\tilde{h}}{\partial \tilde{x}} = \tilde{v}_s(\tilde{E} - \tilde{D}) \tag{3}$$

where \tilde{v}_s is the falling velocity of suspended sediment, \tilde{D} is the deposition rate of suspended sediment ($\tilde{D} = r_0 \tilde{C}$, r_0 is the ratio of the deposition rate to the layer-integrated suspended sediment concentration \tilde{C}). The parameter r_0 is close to unity, assuming it is unity for simplicity in this study. The entrainment rate of sediment from the bottom \tilde{E} is assumed in the form

$$\tilde{E} = \begin{cases} \alpha(\tilde{\tau}_b - \tilde{\tau}_{th})^\gamma & \tilde{\tau}_b \geq \tilde{\tau}_{th} \\ 0 & \tilde{\tau}_b < \tilde{\tau}_{th} \end{cases} \tag{4}$$

where $\tilde{\tau}_{th}$ is the threshold bed shear stress below which erosion does not occur, and the parameters α and γ are empirical constants determined by experiments. The Exner equation describing the mass balance between sediment transported and sediment on the bed takes the form

$$(1 - \lambda_p) \frac{\partial \tilde{\eta}}{\partial \tilde{t}} = \tilde{v}_s (\tilde{D} - \tilde{E}) \tag{5}$$

where λ_p is the porosity of the ocean floor, and \tilde{t} is time.

In the above formulation, we apply the quasi-steady approximation and drop the temporal terms in Equations (1)–(3). The time change of the flow is much swifter than the bed elevation due to sediment transport. Therefore, we can assume that the flow adjusts immediately compared to the bed morphology. Thus, we can assume that the flow is steady and consider the time derivative only in the Exner Equation (5). This approximation is justified in the case of cyclic steps formed by turbidity currents considered in this study.

2.1.2. Normalization

We introduce the normalizations of the form

$$\tilde{U} = \tilde{U}_n U, \quad \tilde{C} = \tilde{C}_n C, \quad \tilde{E} = \tilde{E}_n E, \quad \tilde{D} = \tilde{D}_n C, \tag{6a}$$

$$(\tilde{h}, \tilde{\eta}) = \tilde{H}_n (h, \eta), \quad \tilde{x} = \frac{\tilde{H}_n}{c_D} x, \quad \tilde{t} = \frac{(1 - \lambda_p) \tilde{H}_n}{\tilde{v}_s \tilde{D}_n} t \tag{6b}$$

where the subscript n denotes variables in the equilibrium normal flow condition in the absence of steps. With the aid of Equations (6a) and (6b), the governing Equations (1)–(3) and (5) are rewritten, respectively, in the form

$$U \frac{\partial U}{\partial x} = Ri_n \left(-\frac{1}{2} h \frac{\partial C}{\partial x} - C \frac{\partial h}{\partial x} - C \frac{\partial \eta}{\partial x} + \sigma C \right) - \frac{U^2}{h} \tag{7}$$

$$\frac{\partial U h}{\partial x} = 0 \tag{8}$$

$$\beta \frac{\partial U C h}{\partial x} = E - C \tag{9}$$

$$\frac{\partial \eta}{\partial \tilde{t}} = C - E \tag{10}$$

where β is a non-dimensional parameter representing the suspendability of sediment, σ is the normalized slope, and Ri_n is the Richardson number in the normal flow condition in the absence of steps, which read, respectively

$$\beta = \frac{c_D \tilde{U}_n \tilde{C}_n}{\tilde{v}_s \tilde{D}_n}, \quad \sigma = \frac{S}{c_D}, \quad Ri_n = \frac{Rg \tilde{H}_n \tilde{C}_n}{\tilde{U}_n^2} \tag{11}$$

In the equilibrium normal flow condition, since the gravity force is in balance with the bed shear stress ($\tau_b = \rho RgS\tilde{H}_n$), there is a relationship between the Richardson number Ri_n and σ , where $Ri_n = 1/\sigma$.

The normalized erosion rate of suspended sediment is

$$E = \begin{cases} \left(\frac{U^2 - U_{th}^2}{1 - U_{th}^2} \right)^\gamma & U \geq U_{th} \\ 0 & U < U_{th} \end{cases} \tag{12}$$

where U_{th} is the non-dimensional threshold velocity for entrainment ($=\tilde{U}_{th}/\tilde{U}_n$), and \tilde{U}_{th} is the dimensional threshold velocity for entrainment ($=\sqrt{\tilde{\tau}_{th}/(\rho c_D)}$).

As reported by Taki and Parker et al. [1], the cyclic steps can reach an equilibrium state at which a periodic wave train migrates upstream without changing its form. We introduce the moving coordinates of the form

$$\hat{x} = x + ft, \quad \hat{t} = t \tag{13}$$

where f is the migration speed. Once the cyclic steps reach equilibrium, the average bed slope, wavelength, wave height, and wave migration speed attain constant values. When viewed in the moving coordinates, the deviation of the bed elevation becomes a function of \hat{x} alone. We apply the coordinate transformation described by the above equations to the governing Equations (7)–(10) and drop the hat for simplicity. The Exner Equation (10) reduces to

$$f \frac{d\eta}{dx} = C - E \tag{14}$$

With the aid of Equations (8)–(10), Equation (7) reduces to

$$\frac{dU}{dx} = \frac{\left(\frac{C}{f} - \frac{1}{2U\beta}\right)(E - C) + \sigma C - \frac{U^3}{Ri_n}}{\frac{U}{Ri_n} - \frac{C}{U^2}} \tag{15}$$

The dispersion/diffusion equation of suspended sediment takes the form

$$\frac{dC}{dx} = \frac{E - C}{\beta} \tag{16}$$

2.1.3. Boundary Conditions

The Richardson number is the key to the emergence of cyclic steps. The Richardson critical point stands for a location where the Richardson number is unity. This point divided the flow into the supercritical and subcritical regimes. A hydraulic jump occurs when the currents transit from the supercritical flow to the subcritical one, as shown in Figure 2. If the flow velocity does not reduce to the threshold value for bed erosion, bed erosion will continue, and the periodic cyclic steps will not form. We thus have the additional boundary condition written in the form

$$U_+ = U_{th} \tag{17}$$

The momentum conserves between the upstream and downstream of a hydraulic jump, such that

$$\rho \tilde{U}_-^2 \tilde{h}_- + \frac{1}{2} \rho g R \tilde{C}_- \tilde{h}_-^2 = \rho \tilde{U}_+^2 \tilde{h}_+ + \frac{1}{2} \rho g R \tilde{C}_+ \tilde{h}_+^2 \tag{18}$$

where the subscripts $-$ and $+$ denote variables, respectively, at the upstream and downstream of a hydraulic jump. The suspended sediment concentration is continuous between the upstream and downstream of a hydraulic jump, such that.

$$C_- = C_+ \tag{19}$$

After further manipulation with the use of Equation (19), Equation (18) reduces to

$$U_- = U_{th} \frac{Ri_n + \sqrt{Ri_n^2 + 8Ri_n U_{th}^3 / C_+}}{4U_{th}^3 / C_+} \tag{20}$$

Since the average bed slope does not change even after the formation of steps, we obtain one additional condition of the form

$$\eta_+ = \eta_- = 0 \tag{21}$$

By the use of Equations (14) and (16), the bed elevation η can also be expressed in the form

$$\eta = \frac{\beta}{f}(C_+ - C) = \frac{\beta}{f}(C_- - C) \tag{22}$$

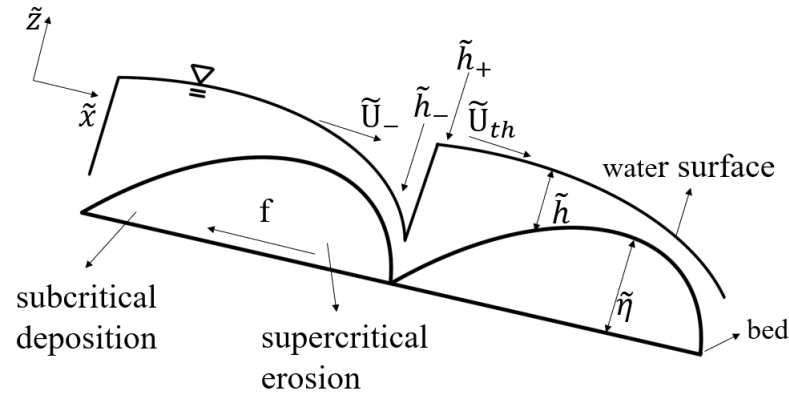


Figure 2. Conceptual sketch of cyclic steps.

2.2. Solution

Solution Method

The governing Equations (15) and (16) with the boundary conditions (19) and (20) form a two-point boundary value problem, which we solve by the shooting method with the Newton–Raphson scheme. Since the problem is similar to that solved by Sun and Parker [6], we follow their solution method to some extent.

The denominator of Equation (15) vanishes at the Richardson critical point. In order to avoid this singularity, the numerator should also vanish at the Richardson critical point. Applying this additional condition, we find the relationship among the critical velocity, the critical suspended sediment concentration, and the migration speed in the form

$$C_c = \frac{U_c^3}{Ri_n} \tag{23}$$

$$f = \frac{2C_c U_c Ri_n \beta (E_c - C_c)}{2U_c \beta (U_c^3 - \sigma C_c Ri_n + Ri_n (E_c - C_c))} \tag{24}$$

where the subscript c denotes variables at the Richardson critical point.

Moreover, L’Hopital’s rule is applied to Equation (15) to calculate dU/dx at the Richardson critical point. Since the flow is accelerating from the subcritical to supercritical regimes via the Richardson critical point, dU/dx should always be positive in order to achieve a physically realistic flow. This condition and some other restrictions allow us to find the solution domain, but since our concern is to find the actual scales of cyclic steps in this paper, we will not go further into this problem. Sun and Parker [6] have further discussed the solution domain. Readers can refer to their study for further information.

Using the Runge–Kutta method, we integrate Equations (15) and (16) in the upstream and downstream directions from the Richardson critical point. Since it is impossible to start a calculation from exactly the Richardson critical point, we use dU/dx and dC/dx to calculate from the vicinity of the Richardson critical point. We guess U_c as the initial value at the Richardson critical point in the integration. Then C_c is determined from Equation (23). While, in the downstream direction, we calculate up to the point where Equation (17) is satisfied, in the upstream direction, we calculate up to the point where Equation (20) is satisfied. These points are where the hydraulic jump takes place, and Equation (19) must be satisfied. We adjust the guessed value of U_c using the Newton–Raphson scheme for Equation (19) to be satisfied and obtain the correct U_c .

For the calculation, it is necessary to specify the parameters β and Ri_n . The parameter β represents the suspendability of sediment in the absence of steps ($=\tilde{u}_n^* \sqrt{c_D} / \tilde{v}_s$), where \tilde{u}_n^*

is the friction velocity in the absence of steps ($=\sqrt{\tilde{\tau}_{bn}/\rho}$). Akiyama and Stefan [18] reported that $\tilde{u}_n^*/\tilde{v}_s$ is larger than unity when suspension starts to occur and takes a value between 50 and 100 when the suspension is saturated. The drag coefficient c_D ranges from 0.002 to 0.02 according to Parker et al. [19]. It follows that the parameter β ranges from 0.04 to 17.32. According to Sun and Parker [6], the flatbed becomes unstable only when the flow is in the supercritical regime. Therefore, the Richardson number has to be smaller than unity. Thus, the possible range of the Richardson number is from zero to unity.

3. Results

The Wavelength as a Function of Ri_n and β

Figure 3 shows the wavelength of cyclic steps as a function of the Richardson number Ri_n and the suspendability β . The wavelength of cyclic steps defines as the distance between two adjacent hydraulic jumps. In the analysis in this study, we obtain the wavelength as the sum of the distances from the Richardson critical point to the downstream and upstream hydraulic jumps, respectively.

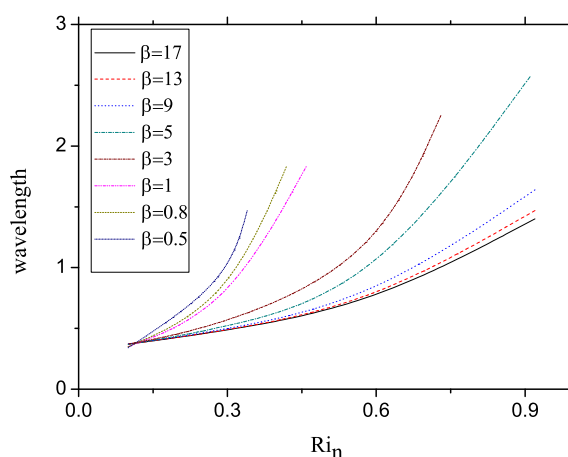


Figure 3. The relationships among typical parameters.

In the calculation, if Ri_n is greater than a specific value or β is smaller than a particular value, the numerator of the equation vanishes at another point other than the Richardson critical point. It is impossible to avoid the two singularities simultaneously. In this sense, we can see that the model proposed here has no solution when β is smaller than 0.12. It means that if β is smaller than a certain threshold, a cyclic step will not form regardless of the value of β , since the large suspendability and the generation of abundant suspended sediment are essential for the formation of cyclic steps.

In addition, we find that, as the suspendability decreases, steps will not form unless the slope is considerably steep, and if the suspendability is sufficiently large, cyclic steps can appear even on mild slopes. The analysis also shows that cyclic steps with relatively long wavelengths appear on mild slopes, while those with short wavelengths form on steep slopes. This tendency may be because, on steep slopes, the flow variation is generally rapid, and the intervals between hydraulic jumps decrease. We also find that large suspendability leads to short wavelengths. The reason may be that when the suspendability is more prominent, fewer suspended particles settle out of the fluid to form cyclic steps.

4. Discussion

Application

The non-dimensional step wavelength and wave height are obtained as functions of Ri_n and β . These two parameters can be calculated by the drag coefficient c_D , bed slope S , and the value of $\tilde{u}_n^*/\tilde{v}_s$. The wave height is the distance between the highest point of a crest and the bed. Since the wave height is normalized by the dimensional layer thickness of

turbidity currents in the absence of steps \tilde{H}_n and the wavelength is normalized by \tilde{H}_n/c_D , \tilde{H}_n is estimated to obtain the actual scales of cyclic steps.

Typical values for parameters were taken from cyclic steps within the South Taiwan Shoal canyon [9] to reproduce the submarine cyclic steps (Figure 4). We assume c_D is 0.003. Ri_n can be calculated with the aid of an average slope of 0.27 in the upper segment and 0.66 in the lower segment ($Ri_n = c_D/S$). The value of $\tilde{u}_n^*/\tilde{v}_s$ is assumed to be 10, and thus β is 0.55 ($\beta = \tilde{u}_n^*\sqrt{c_D}/\tilde{v}_s$).

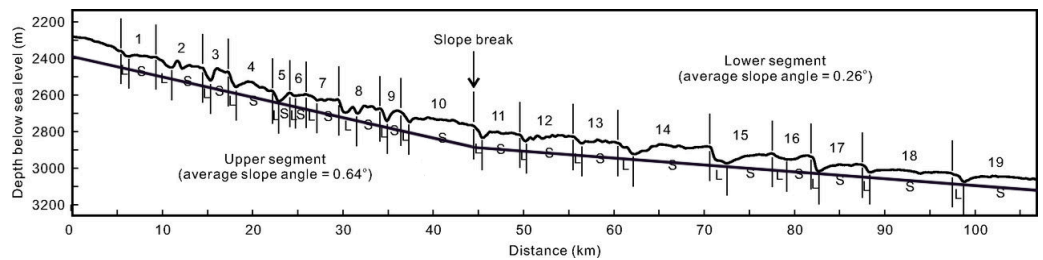


Figure 4. Cyclic steps within the South Taiwan Shoal canyon. Redrafted from Zhong et al. [9]. 1–10 cyclic steps are in the upper segment and 11–19 cyclic steps are in the lower segment; L indicates the lee sides and S indicates the stoss sides.

To achieve the estimation of the layer thickness of long-runout turbidity currents in the absence of steps, we employ the following relation proposed by Izumi [17]:

$$\frac{\tilde{H}_n}{\tilde{D}_s} = \frac{R_f^2 \cdot C_b(v_s)}{v_s^2 \cdot S \cdot E_n} \tag{25}$$

Here R_f is the falling velocity normalized by the sediment diameter ($=\tilde{v}_s/\sqrt{Rg\tilde{D}_s}$), \tilde{D}_s is the sediment diameter, C_b is the suspended sediment concentration near the bottom normalized by the layer averaged suspended sediment concentration, and v_s is the falling velocity normalized by the friction velocity ($=\tilde{v}_s/\tilde{u}_n^*$). Assuming that \tilde{D}_s is 0.4 mm herein, we find R_f 0.4. As for the entrainment rate of sediment from the bottom in the equilibrium condition in the absence of steps \tilde{E}_n , Izumi and Fujii [20] proposed a formula of the form

$$\tilde{E}_n = K \left[\left(\frac{\tilde{u}_n^*}{\tilde{v}_s} \right)^2 - 1 \right]^m \tag{26}$$

where K and m are constants that need to be determined empirically, and assumed to be 2×10^{-5} and 2, respectively. Assuming $\tilde{u}_n^*/\tilde{v}_s$ to be 10 as already mentioned, we find \tilde{E}_n to be 0.2. With the use of the above assumptions, we find that the thickness of the highly concentrated layer is 20.05 m and 49.36 m in the upper and lower segment, respectively.

We can calculate the real scales of wavelength and wave height with the aid of Equation (6b). It should note that the wavelength and wave height of cyclic steps obtained in the analysis are in good agreement with the field observations. According to Zhong et al. [9], the range of wave heights is 15 m to 81 m within the South Taiwan Shoal canyon. The wavelengths of cyclic steps range from 1800 m to 8414 m in the upper segment and 4078 m to 10,452 m in the lower segment. Our model results show that the wavelength is 2135.17 m, and the wave height is 25.57 m in the upper segment. In the lower segment, the wavelength is 5686.29 m, and the wave height is 26.30 m.

The steps in the lower segment are relatively longer than those in the upper segment, and it also concurs with observations within the South Taiwan Shoal canyon. Additionally, the wavelength of cyclic steps is some orders of magnitude larger than the layer thickness, so the long wave assumption is satisfied.

Using the present model, we obtain the bed profiles over a one-step wavelength in both the upper and lower segments within the South Taiwan Shoal canyon. Figures 5 and 6 show the bed and water surface profiles of one step with the aid of Equation (22), where

$\tilde{\zeta} = \tilde{\eta} + \tilde{h}$ and the Richardson critical point is at $\tilde{x} = 0$. Observed appearances bear a good agreement with the steps reproduced by the model.

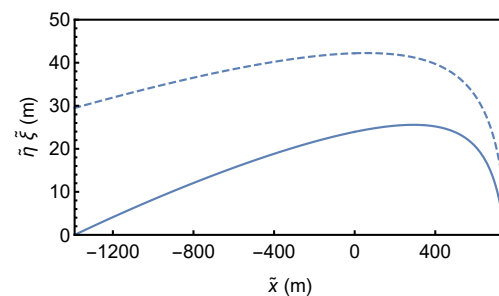


Figure 5. The distributions of non-normalized bed elevation and water surface over one step wavelength, in the upper segment.

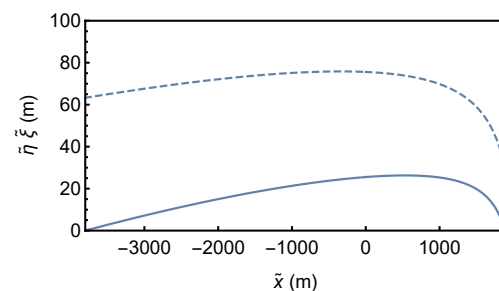


Figure 6. The distributions of non-normalized bed elevation and water surface over one step wavelength, in the lower segment.

5. Conclusions

We present an analytical model to reproduce the cyclic steps of long-runout turbidity currents. Since the lower layer is the focus of this analysis, the entrainment from ambient seawater is considered negligible. Using the model proposed in this study, we can predict the dimensions of cyclic steps observed in the field. The analytical results show that cyclic steps cannot form when β (suspendability) or the average slope divided by the drag coefficient is smaller than some threshold. Furthermore, the wavelengths of cyclic steps on mild slopes were relatively long, while the larger slope angle facilitates the formation of relatively short wavelengths. The results of the analysis are consistent with field observations.

Author Contributions: Conceptualization, Z.W. and N.I.; methodology, Z.W. and N.I.; writing—original draft preparation, Z.W.; writing—review and editing, N.I. All authors have read and agreed to the published version of the manuscript.

Funding: This research was funded by Hokkaido University Ambitious Doctoral Fellowship (SDGs), grant number JPMJFS2101.

Institutional Review Board Statement: Not applicable.

Informed Consent Statement: Not applicable.

Data Availability Statement: Not applicable.

Acknowledgments: We thank all the members of the River and Watershed Laboratory for their support and helpful suggestions.

Conflicts of Interest: The authors declare no conflict of interest. The funders had no role in the design of the study; in the collection, analyses, or interpretation of data; in the writing of the manuscript, or in the decision to publish the results.

Notation

B	empirical constant ($=1.3 \times 10^{-7}$)
C	suspended sediment concentration (–)
C_b	suspended sediment concentration near bed (–)
D	deposition rate of suspended sediment (–)
\bar{D}_s	sediment size (mm)
E	entrainment rate of suspended sediment (–)
K	empirical constant ($=2 \times 10^{-5}$)
R	submerged specific gravity (–)
S	average slope (–)
U	mean velocity in x direction (–)
U_{th}	threshold velocity below which erosion does not occur (–)
α	empirical constant determined by experiments (–)
e_w	entrainment of water (–)
f	migration speed (–)
g	gravity acceleration (m s^{-2})
h	highly concentrated layer thickness of turbidity currents (–)
m	empirical constant ($=2$)
t	time (–)
u_n^*	friction velocity (–)
v_s	falling velocity (–)
x	streamwise coordinate (–)
z	upward coordinate (–)
R_f	normalized fall velocity (–)
R_i	Richardson number (–)
R_p	particle Reynolds number (–)
β	a nondimensional parameter representing the suspendability of the turbidity currents (–)
η	the bed elevation referenced to the average bed slope (–)
λ_p	porosity of sediment (–)
γ	empirical constant determined by experiments (–)
r_0	the ratio between the suspended sediment concentrations and \tilde{C} (–)
ρ	density of water (kg m^{-3})
τ_b	bed shear stress (–)
ζ	water surface elevation (–)
$()_n$	for the case of normal flow in the absence of steps
$(\tilde{ })$	dimensional variables

References

1. Taki, K.; Parker, G. Transportational cyclic steps created by flow over an erodible bed. Part 1. Experiments. *J. Hydraul. Res.* **2005**, *43*, 488–501. [\[CrossRef\]](#)
2. Fildani, A.; Normark, W.R.; Kostic, S.; Parker, G. Channel formation by flow stripping: Large-scale scour features along the Monterey East Channel and their relation to sediment waves. *Sedimentology* **2006**, *53*, 1265–1287. [\[CrossRef\]](#)
3. Pirmez, C.; Imran, J. Reconstruction of turbidity currents in Amazon Channel. *Mar. Pet. Geol.* **2003**, *20*, 823–849. [\[CrossRef\]](#)
4. Urgeles, R.; Cattaneo, A.; Puig, P.; Liqueste, C.; De Mol, B.; Amblas, D.; Sultan, N.; Trincardi, F. A review of undulated sediment features on Mediterranean prodeltas: Distinguishing sediment transport structures from sediment deformation. *Mar. Geophys. Res.* **2011**, *32*, 49–69. [\[CrossRef\]](#)
5. Smith, I.B.; Holt, J.W.; Spiga, A.; Howard, A.D.; Parker, G. The spiral troughs of Mars as cyclic steps. *J. Geophys. Res. Planets* **2013**, *118*, 1835–1857. [\[CrossRef\]](#)
6. Sun, T.; Parker, G.; Izumi, N. Transportational cyclic steps created by flow over an erodible bed. Part 2. Theory and numerical simulation. *J. Hydraul. Res.* **2005**, *43*, 502–514. [\[CrossRef\]](#)
7. Parker, G.; Izumi, N. Purely erosional cyclic and solitary steps created by flow over a cohesive bed. *J. Fluid Mech.* **2000**, *419*, 203–238. [\[CrossRef\]](#)
8. Spinewine, B.; Sequeiros, O.E.; Garcia, M.H.; Beaubouef, R.T.; Sun, T.; Savoye, B.; Parker, G. Experiments on wedge-shaped deep sea sedimentary deposits in minibasins and/or on channel levees emplaced by turbidity currents. Part II. Morphodynamic evolution of the wedge and of the associated bedforms. *J. Sediment. Res.* **2009**, *79*, 608–628. [\[CrossRef\]](#)
9. Zhong, G.; Cartigny, M.J.; Kuang, Z.; Wang, L. Cyclic steps along the South Taiwan Shoal and West Penghu submarine canyons on the northeastern continental slope of the South China Sea. *Bulletin* **2015**, *127*, 804–824. [\[CrossRef\]](#)

10. Izumi, N.; Yokokawa, M.; Parker, G. Incisional cyclic steps of permanent form in mixed bedrock-alluvial rivers. *J. Geophys. Res. Earth Surf.* **2017**, *122*, 130–152. [[CrossRef](#)]
11. Dias, D.; Izumi, N.; Yokokawa, M. Cyclic steps formed by turbidity currents. *J. Jpn. Soc. Civ. Eng. Ser. A2 (Appl. Mech. (AM))* **2011**, *67*, 503–510. [[CrossRef](#)]
12. Parker, G.; Fukushima, Y.; Pantin, H.M. Self-accelerating turbidity currents. *J. Fluid Mech.* **1986**, *171*, 145–181. [[CrossRef](#)]
13. Izumi, N. The formation of submarine gullies by turbidity currents. *J. Geophys. Res. Ocean.* **2004**, *109*, C03048. [[CrossRef](#)]
14. Luchi, R.; Balachandar, S.; Seminara, G.; Parker, G. Turbidity currents with equilibrium basal driving layers: A mechanism for long runout. *Geophys. Res. Lett.* **2018**, *45*, 1518–1526. [[CrossRef](#)]
15. Paull, C.K.; Talling, P.J.; Maier, K.L.; Parsons, D.; Xu, J.; Caress, D.W.; Gwiazda, R.; Lundsten, E.M.; Anderson, K.; Barry, J.P.; et al. Powerful turbidity currents driven by dense basal layers. *Nat. Commun.* **2018**, *9*, 4114. [[CrossRef](#)]
16. Pope, E.L.; Cartigny, M.J.; Clare, M.A.; Talling, P.J.; Lintern, D.G.; Vellinga, A.; Hage, S.; Acikalin, S.; Bailey, L.; Chapplow, N.; et al. First source-to-sink monitoring shows dense head controls sediment flux and runout in turbidity currents. *Sci. Adv.* **2022**, *8*, eabj3220. [[CrossRef](#)] [[PubMed](#)]
17. Izumi, N. Equilibrium thickness of the highly concentration layer formed at lower turbidity currents. *J. Jpn. Soc. Civ. Eng. Ser. B1 (Hydraul. Eng.)* **2018**, *74*, 811–816.
18. Akiyama, J.; Stefan, H.; Henry M. Turbidity current with erosion and deposition. *J. Hydraul. Eng.* **1985**, *111*, 1473–1496. [[CrossRef](#)]
19. Parker, G.; Garcia, M.; Fukushima, Y.; Yu, W. Experiments on turbidity currents over an erodible bed. *J. Hydraul. Res.* **1987**, *25*, 123–147. [[CrossRef](#)]
20. Izumi, N.; Fujii, K. Channelization on plateaus composed of weakly cohesive fine sediment. *J. Geophys. Res. Earth Surf.* **2006**, *111*, F01012. [[CrossRef](#)]